Published in final edited form as:
Angiogenesis. 2011 December ; 14(4): 491–501. doi:10.1007/s10456-011-9233-1.

Monitoring Antivascular Therapy in Head and Neck Cancer Xenografts using Contrast-enhanced MR and US Imaging

Mukund Seshadri[1,2], **Nuno T. Sacadura**[3], and **Tonya Coulthard**[3]

[1]Department of Pharmacology and Therapeutics (Preclinical Imaging Laboratory), Roswell Park Cancer Institute, Buffalo, New York

[2]Department of Dentistry and Maxillofacial Prosthetics, Roswell Park Cancer Institute, Buffalo, New York

[3]VisualSonics Inc., Toronto, Ontario

Abstract

Background—The overall goal of this study was to non-invasively monitor changes in blood flow of squamous cell carcinoma of the head and neck (SCCHN) xenografts using contrast-enhanced magnetic resonance (MR) and ultrasound (US) imaging.

Methods—Experimental studies were performed on mice bearing FaDu tumors and SCCHN xenografts derived from human surgical tissue. MR examinations were performed using gadofosveset trisodium at 4.7T. Change in T1-relaxation rate of tumors (ΔR1) and tumor enhancement parameters (amplitude, area under the curve - AUC) were measured at baseline and 24 hours after treatment with a tumor-vascular disrupting agent (tumor-VDA), 5,6-dimethylxanthenone-4-acetic acid (DMXAA; ASA404) and correlated with tumor necrosis and treatment outcome. CE-US was performed using microbubbles (Vevo MicroMarker®) to assess the change in relative tumor blood volume following VDA treatment.

Results—A marked decrease (up to 68% of baseline) in T1-enhancement of FaDu tumors was observed one day after VDA therapy indicative of a reduction in blood flow. Early (24h) vascular response of individual tumors to VDA therapy detected by MRI correlated with tumor necrosis and volume estimates at 10 days post treatment. VDA treatment also resulted in a significant reduction in AUC and amplitude of patient tumor-derived SCCHN xenografts. Consistent with MRI observations, CE-US revealed a significant reduction in tumor blood volume of patient tumor-derived SCCHN xenografts after VDA therapy. Treatment with VDA resulted in a significant tumor growth inhibition of patient tumor derived SCCHN xenografts.

Conclusions—These findings demonstrate that both CE-MRI and CE-US allow monitoring of early changes in vascular function following VDA therapy. The results also demonstrate, for the first time, potent vascular disruptive and antitumor activity of DMXAA against patient tumor-derived head and neck carcinoma xenografts.

Keywords

Angiogenesis; SCCHN; VDAs; MRI; US

Address correspondence to: Dr. Mukund Seshadri, Mukund.Seshadri@roswellpark.org Ph: 716-845-1552; Fax: 716-845-8857..

Disclosure of Potential Conflicts of Interest: Seshadri M – None
Sacadura NT and Coulthard T are full-time employees of VisualSonics Inc.

INTRODUCTION

Squamous cell carcinomas are among the most common type of neoplasms of the upper aerodigestive tract in humans [1]. While squamous cell carcinomas of the head and neck (SCCHN) constitute a biologically diverse set of neoplasms, angiogenesis is an early and essential step in head and neck carcinogenesis [2, 3]. Tumor vascularity has a strong influence on disease progression and therapeutic response in SCCHN [4, 5]. As a result, several preclinical and clinical studies have examined and successfully demonstrated the potential of angiogenesis inhibitors (AIs) alone and in combination with chemotherapy against head and neck cancers [6-9]. However, the therapeutic potential of tumor vascular disrupting agents (VDAs), a relatively new class of agents that cause disruption of existing tumor vasculature [10], has not been extensively evaluated against SCCHN.

The development of AIs and VDAs has led to a renewed interest in the use of functional imaging methods to study tumor angiogenesis in both preclinical models and in patients enrolled in clinical trials [11, 12]. Ex-vivo analytical techniques such as immunostaining of tissue sections and gene expression arrays provide useful molecular information relating to tumor vascular biology. However, their invasive nature precludes monitoring of temporal and spatial changes occurring within the tumor microenvironment. In contrast, imaging techniques such as magnetic resonance imaging (MRI), positron emission tomography (PET), computed tomography (CT) and ultrasound (US) provide opportunities for non-invasive, longitudinal assessment of tumor pathophysiology in experimental models and in patients. In addition to providing three-dimensional morphologic assessment of macroscopic tumor size/volume, imaging methods can provide quantitative estimates of parameters relating to tumor cellular and vascular function such as cell death/necrosis, blood flow and vascular permeability [11-14]. One such imaging method that has been widely used to characterize tumor microvasculature in living subjects and to monitor changes in tumor vascular function following treatment is dynamic contrast-enhanced MRI (DCE-MRI) [12]. Most DCE-MRI studies are based on serial imaging of changes in signal intensity within a given tissue of interest (tumor) before and after intravenous administration of a contrast-enhancing agent, typically containing gadolinium [11, 12]. Pharmacokinetic analysis of these dynamic datasets is then performed to relate the contrast agent distribution within the tissue to physiological parameters such blood flow, vascular surface area and vessel leakiness [11-13].

In this study, we utilized dynamic contrast-enhanced MRI to study the microvascular characteristics of SCCHN xenografts established in immunodeficient mice. Studies were performed on nude/SCID mice bearing SCCHN xenografts obtained by transplantation of (a) FaDu, a poorly differentiated SCCHN cell line, and, (b) primary SCCHN xenografts derived from surgical specimens obtained from patients [15]. Dynamic contrast-enhanced MRI examinations were performed using the clinically approved gadolinium-based contrast agent, gadofosveset trisodium (Ablavar™; Vasovist). In addition to MRI, contrast-enhanced ultrasound (CE-US) [16] was employed to determine the effects of VDA therapy on patient tumor-derived SCCHN xenografts. CE-US imaging was chosen as it offers a relatively inexpensive alternative to MRI and CT and can also provide quantitative estimates of blood perfusion [16, 17].

The overall goal of the study was to examine the potential of MRI and US for non-invasive monitoring of early changes in tumor blood flow following VDA therapy *in vivo* and to demonstrate the activity of VDA therapy against SCCHN.

MATERIALS AND METHODS

Animals

Female athymic nude mice (foxn1/nu, body weight 20-25 g) were obtained from Harlan Sprague Dawley, Inc. (Indianapolis, IN) and severe combined immunodeficient (SCID) mice were bred in house within the Laboratory Animal Resource at Roswell Park Cancer Institute. Animals were housed in microisolator cages, provided standard chow/water and maintained on 12-hour light/dark cycles in an HEPA-filtered environment.

Tumor model system

Studies were carried out using two different SCCHN xenografts, (i) FaDu – human hypopharyngeal squamous cell carcinomas established in athymic nude mice, and, (ii) surgical SCCHN tissue implanted into SCID mice. All surgical procedures relating to tumor implantation were performed under sterile conditions, with animals anesthetized using the inhalational anesthetic, Isoflurane (3% in oxygen, Abbott Laboratories, IL), in a laminar flow hood. For establishment of FaDu tumors, approximately 1×10^6 cells of human FaDu squamous cell carcinoma were initially implanted subcutaneously into the flanks of donor mice. Upon reaching a volume of ~500-1000 mm^3, animals were euthanized and tumors harvested and sectioned into 1-2 mm fragments for transplantation into recipient mice.

Patient tumor-derived SCCHN xenografts were established by subcutaneous transplantation of small fragments of surgical tumor tissue using a trocar under aseptic conditions as described previously [15]. Tissue specimens were obtained from patients following written consent and under a research protocol approved by the Institutional Review Board and the research ethics committee. A triple antibiotic ointment (VWR International, West Chester, PA) was applied to the site of trocar entry to prevent any wound infection. All surgical procedures on mice were performed as outlined in protocols approved by the Institutional Animal Care and Use Committee (IACUC).

Magnetic resonance imaging

MRI examinations were carried out in a 4.7 T/33-cm horizontal bore magnet (GE NMR Instruments, Fremont, CA) incorporating AVANCE digital electronics (Bruker Biospec with ParaVision 3.0.2; Bruker Medical Inc., Billerica, MA) and a removable gradient coil insert (G060, Bruker Medical Inc., Billerica, MA) generating maximum field strength of 950 mT/m and a custom-designed 35-mm RF transmit-receive coil. For *in vivo* imaging, tumor-bearing animals were anesthetized using Isoflurane (Abbott Laboratories, IL), induced at 3-3.5% in oxygen, and sustained 2-2.5% during imaging. The mice were secured in a form-fitted, MR compatible sled (Dazai Research Instruments, Toronto, Canada) equipped with temperature and respiratory monitoring sensors. The sled, along with a phantom containing 0.15 mM gadopentetate dimeglumine (Gd-DTPA; Magnevist, Berlex Laboratories, Wayne, NJ) was then positioned inside the scanner using a plastic carrier tube. Animal body temperature was maintained at 37°C during imaging using an air heater system (SA Instruments Inc., Stony Brook, NY), and automatic temperature feedback was initiated through thermocouples in the sled, in conjunction with computer software supplied with the heater.

Data acquisition consisted of localizer images, T2-weighted (T2W) and T1-weighted (T1W) spin echo (SE) images**.** Axial T2W images of the tumor were acquired with the following parameters: FOV = 3.20 × 3.20 cm, matrix = 192 × 192, slice thickness = 1.00 mm, interslice distance = 1.25 mm, NEX = 2, TR = 2793 ms, and TE_{eff} = 15.0 ms. T1-mapping of tumors was performed using a saturation recovery fast spin echo (T1-FSE) sequence with the following parameters: FOV = 3.20 × 3.20 cm, MTX = 128 × 96, NEX = 1, slice

thickness = 1.00 mm, number of slices = 5, interslice distance = 1.25 mm, RARE/Echoes = 8/8, TE_{eff} = 25 ms and TR = 6000, 3000, 1500, 750, 500, 360.34 ms. Single slice T1-mapping of blood (vena cava) was performed using a Fast Imaging with Steady-State Precession (True-FISP) sequence using the following parameters: FOV = 3.20 × 3.20 cm, MTX = 128 × 128, TR/ TE_{eff}. = 3.0/1.5 ms, NEX = 1, slice thickness = 1.50 mm, TI = 40.0 ms, flip angle = 60°, number of frames = 100, number of segments = 16 [15]. The contrast enhanced MRI protocol consisted of three pairs of alternating T1-FSE and True-FISP scans to quantify T1-relaxation measurements of tumor and blood before contrast agent injection. Following completion of precontrast scans, gadofosveset (Ablavar; Lantheus Medical Imaging, N. Billerica, MA) was administered intravenously (0.1 mmol Gd/kg) through the lateral tail vein following which a second set of five alternating pairs of T1-FSE and True-FISP scans were acquired to quantify changes in T1-relaxation post-contrast out to ~50 minutes post-injection.

Post processing and MR Image analysis

Following image acquisition, raw image sets were transferred to a processing workstation and converted into Analyze™ format (AnalyzeDirect, version 7.0; Overland Park, KS). All post processing of imaging data was carried out in Analyze™ and MATLAB (Mathworks Inc, Natick, MA). For vascular response assessment studies, a region of interest (ROI) was traced around the entire tumor area on each tumor slice excluding the surrounding skin on T2 weighted images and saved as an object map. The object map was then transferred onto the T1-weighted images acquired with the same slice prescription. Signal intensities from ROIs were obtained and mean intensity within the ROIs was used for calculating the T1-relaxation at each TR time. The relaxation rate R1 and the maximal signal intensity S_{max} were then obtained by non-linear fitting of the equation, using Matlab's curve-fitting toolbox (Matlab 6.5; Mathworks Inc., Natick, MA), following subtraction of background noise

$$S_{TR} = S_{max}\left(1 - e^{-(R1^{*}TR)}\right)$$

where S_{TR} is the signal intensity obtained at each TR time. The change in R1 (ΔR1) values were calculated for the tumor and the blood (vena cava) by subtracting the mean precontrast R1 values from each post contrast R1 measurement. The time of intravenous administration of the contrast agent (gadofosveset) was designated as t = 0. Times of all post contrast scans were calculated from the time of contrast agent injection and used to report the change in R1 over time. The ΔR1 versus time curve was used to calculate area under the curve (AUC) and the maximum amplitude of enhancement defined as the maximum ΔR1 value obtained following contrast. R1 maps were calculated on a pixel-by-pixel basis in MATLAB and color lookup table was applied.

Ultrasound imaging

Ultrasound imaging was performed using the Vevo 2100 high-frequency ultrasound system (VisualSonics, Toronto, ON, Canada). Tumor-bearing mice were anesthetized with Isoflurane (Benson Medical Industries, Markham, ON, Canada) at 1.5% concentration with medical air delivered through a vaporizer. Mice were positioned on a heated platform (THM 150; Indus Instruments, Webster, TX) equipped with integrated temperature sensor and ECG electrodes for imaging. All four paws were secured onto the ECG pads and body temperature was kept between 34 °C and 37 °C. A 27-gauge butterfly needle connected to a 12 cm catheter was inserted into a tail vein for intravenous administration of the contrast agent (Vevo MicroMarker®; VisualSonics, Toronto, Canada). A depilatory cream (Nair, Church and Dwight Canada Corp., Mississauga, ON, Canada) was applied to the skin on the tumor and surrounding regions. An ultrasound acoustic gel (Aquasonic 100, Parker

Laboratories Inc., Fairfield, New Jersey) was applied to facilitate ultrasound transmission from the transducer to the skin. A solid state transducer (MS-250SC) was placed on the tumor and held in position by a clamp mounted on the Vevo Rail System. This transducer has a center frequency of 18 MHz and an axial resolution of 75 μm at an elevation of 8 mm. Nonlinear Contrast Mode imaging was employed to detect the presence of Vevo MicroMarker® contrast agent (VisualSonics, Toronto, ON, Canada). The agent consists of phospholipid shell microbubbles filled with perflurobutane and nitrogen with a diameter ranging from 2.3 to 2.9-μm. A bolus injection of 50 μl (concentration of 2×10^9 microbubbles/ml) was delivered through the tail vein catheter. Nonlinear detection of the contrast signal was done in 3 dimensions by stepping the transducer through the volume of the tumor at a step-size of 0.152 mm. Acquisition parameters were kept constant at 4% power, 28 dB contrast gain, gate size of 6, high line density, and standard beam width. Tumor volume was determined by manually outlining the borders of the tumor in several images throughout the stack acquired in 3D scanning. The percent agent (PA) value was calculated using the Vevo 2100 3D software as the percentage of pixels within the tumor volume that have a nonlinear contrast overlay instead of a gray scale B-mode pixel. Baseline PA values were acquired before contrast agent delivery and compared to PA value after delivery, while the contrast agent circulates through the subcutaneous tumor. A differential PA value was calculated by subtracting the baseline PA from the post-injection PA; this value was used as a measure of relative blood volume [17].

Histology and tumor response assessment

FaDu tumors were harvested for histology following completion of imaging on day 10 post treatment. Sections were stained with Harris haematoxylin (Poly Scientific, Bay Shore, NY) as described previously [15]. Glass slides containing various tissue sections were scanned and digitized using the ScanScope XTsystem (Aperio Technologies, Vista, CA). Digitized images were then captured using the ImageScope software (Version 9.1; Aperio Technologies). Tumor response was evaluated by measuring the change in tumor volume following treatment. Tumor volume was calculated from caliper based measurements of tumor dimensions using the formula, $V = (l \times w^2)/2$, where l – longest dimension of the tumor and w is the axis perpendicular to *l*.

Study design and statistical considerations

Three different experimental imaging studies were performed. (i) DCE-MRI with gadofosveset was performed in nude mice bearing FaDu tumor xenografts before and after VDA treatment (DMXAA; ASA404, 25 mg/kg, n=4). (ii) DCE-MRI of SCID mice bearing patient tumor-derived SCCHN xenografts was performed on untreated controls (n=3) and animals treated with DMXAA (22 mg/kg, n=4) 24 hours after treatment. For therapeutic studies, tumor-bearing mice were injected with the VDA DMXAA at a dose of 22 mg/kg (i.p.) and imaging performed before and 24h after treatment. Tumor response to therapy was evaluated by measuring change in tumor volume between control (n=6) and VDA-treated animals (n=6). (iii) Baseline US images were acquired on 7 animals bearing patient tumor-derived SCCHN xenografts before and after contrast (Vevo MicroMarker®; VisualSonics, Toronto, Canada) agent administration. Data from one animal was discarded due to an experimental error. Four animals were then treated with the VDA DMXAA (25 mg/kg) and contrast-enhanced US imaging repeated at 24 hours post treatment. Response of SCCHN xenografts to VDA therapy was monitored by measuring the change in tumor volume of controls (n=6) and treated (n=5) over a 30-day period following VDA treatment (25 mg/kg, once a week for 3 weeks). Longitudinal tumor growth data were analyzed by ANOVA for repeated measures. When each individual animal served as its own control, differences between baseline and 24h post treatment time points were assessed using the paired two-tailed t test. Statistical analysis and graphical presentation of data was performed using

GraphPad Prism (Version 5.00 for Windows, GraphPad Software, San Diego California USA, www.graphpad.com). Values are reported as mean ± standard error of the mean.

RESULTS

DCE-MRI of FaDu SCCHN xenografts

We first examined the enhancement characteristics of untreated FaDu SCCHN xenografts using gadofosveset (MS-325; Ablavar™). Axial T2-weighted image and corresponding R1 maps of an untreated control FaDu tumor before (*upper*) and after (*lower*) gadofosveset injection is shown in Figure 1. As can be seen from the enlarged image of the ROI, marked contrast enhancement was detected within the tumor particularly in the tumor periphery following gadofosveset administration. We then examined the utility of gadofosveset-enhanced MRI to monitor changes in tumor vascularity following therapeutic intervention. For these studies, tumor-bearing animals were imaged before (day 0) and 24h after treatment (day 1) with a tumor vascular disrupting agent, DMXAA. Tumor T1 measurements (R1 = 1/T1) were obtained before contrast (precontrast) and for approximately 50 minutes after contrast agent administration. Quantitative estimates of the change in R1 post contrast (ΔR1) were obtained and plotted as a function of minutes post injection of gadofosveset after normalization to ΔR1 of blood in the vena cava (Fig 2a). Following VDA therapy (d1), a marked reduction in enhancement (ΔR1) was seen compared to baseline pretreatment values (d0) indicative of tumor vascular disruption. Area under the gadolinium concentration curve (AUGC; Fig 2b) and amplitude (max. ΔR1; Fig 2c) were calculated on both days and analyzed for statistical significance. A significant reduction in AUGC and amplitude was observed on day 1 compared to day 0 values ($p<0.05$). The reduction in AUC and amplitude was consistently observed in all 4 treated tumors (tumor IDs A1-A4).

We then investigated if the early vascular response to VDA therapy detected by MRI correlated with the subsequent outcome of individual tumors. The panel of images shown in Figure 3 represents post contrast R1 maps of two tumors (A1 and A2) on day 0 and day 1. Tumor A1 (76.5 mm^3 on day 0) showed ~68% reduction in AUGC at 24 hours post VDA therapy and was associated with marked tumor growth inhibition (18.9 mm^3 on day 10). Histologic examination of the tumor on day 10 showed extensive areas of necrosis with very few viable areas within the tumor. In contrast, tumor A2 (41.7 mm^3 on day 0) showed only ~35% reduction in AUGC at 24 hours compared to baseline values and was associated with tumor growth (373.7 mm^3 on day 10). Histologic sections of the tumor showed the presence of a viable proliferating tumor mass with minimal areas of necrosis. Histologic sections of all 4 treated tumors are shown in supplementary material (Supp figure S1).

Gadofosveset-enhanced MRI of patient tumor-derived SCCHN xenografts

Next, we investigated the vascular disruptive activity of DMXAA against patient tumor-derived SCCHN xenografts using gadofosveset-enhanced MRI. Figure 4a shows calculated R1 maps of a control and VDA treated SCCHN xenograft before (preGd) and after gadofosveset (postGd) administration. Two contiguous slices showing kidneys (slice 1, *dotted outline*) and tumors (*arrow*) are shown. A marked increase in contrast agent accumulation was visualized on the post contrast R1 maps of control animals. In comparison, DMXAA-treated tumors showed minimal enhancement in contrast following gadofosveset injection. To account for potential differences in contrast agent injection between the two cohorts, ΔR1 values of the tumor were normalized to blood and used to calculated AUGC and amplitude values. A significant reduction in AUGC ($p<0.05$, Fig 4b) and amplitude ($p<0.01$, Fig 4c) was observed 24 hours after VDA therapy compared to untreated controls. Treatment with a single injection of the tumor-VDA resulted in moderate

tumor growth inhibition of patient tumor-derived SCCHN xenografts over a 25 day period (Figure 4d).

Contrast-enhanced US imaging of patient tumor-derived SCCHN xenografts

Finally, we examined the antivascular activity DMXAA on patient tumor-derived SCCHN xenografts using contrast-enhanced ultrasound with non-targeted microbubbles (Vevo MicroMarker®). Increase in the non linear contrast mode signal was used as an estimate of overall tumor vascularity. The panel of images shown in Figure 5 represent images of non linear contrast mode signal (copper overlay) of a control SCCHN xenograft before and after administration of microbubbles. Following administration of the microbubbles, ~50% increase in non linear contrast model signal (Fig 5b; PA = 76.63%) was seen within the tumor compared to precontrast estimates (Fig 5a; PA = 26.62%). Corresponding 3D volume generated for the tumor is shown in Figure 5c (119 mm^3).

Figure 6a shows B-mode and contrast-mode images of a SCCHN xenograft before and after microbubble injection on day 0 (pretreatment) and day 1 (24 hours post therapy). Contrast mode images of the tumor showed a reduction in enhancement following treatment compared to pretreatment images (Fig 6a). Non-linear signal enhancement following contrast was used as a measure of the relative blood volume (rBV) of tumors (Fig 6b). rBV values of control SCCHN xenografts were 48.11 ± 1.4% (n=6). Twenty four hours after VDA therapy, a significant reduction ($p<0.01$) in rBV was observed (23.98 ± 6.7%, n=4). Administration of the VDA (25 mg/kg, once a week x 3) resulted in a marked inhibition of SCCHN tumors and a delay in tumor regrowth *in vivo* as can be seen from the tumor growth curves over a 60 day period (Figure 6c; $p<0.001$).

DISCUSSION

The awareness of angiogenesis as one of the hallmarks of cancer has resulted in the development of a number of therapies targeted towards tumor vasculature [18, 19]. This has also led to a renewed interest in developing non-invasive imaging methods to study tumor angiogenesis in living subjects. Radiologic methods that have traditionally been viewed as a diagnostic tools for visualization of anatomy, have now become integral tools in oncology that enable functional molecular imaging of tumors. In the present study, two such radiologic methods, CE-MRI and CE-US, were utilized to characterize the microvascular characteristics and therapeutic response of SCCHN xenografts.

MRI offers superior contrast for accurate delineation of soft tissues including tumors, cysts and inflammatory lesions in the head and neck region [20]. In clinical oncology, DCE-MRI techniques have been widely used for studying tumor angiogenesis and hypoxia of human tumors [21, 22]. Patterns of signal enhancement and spatial heterogeneities observed following administration of MR contrast-enhancing agents have been used to identify invasive or actively proliferating regions in tumors [23]. DCE-MRI has also been used to classify nodal metastasis and bone invasion in head and neck cancer patients [24, 25]. Changes in blood volume detected by DCE-MRI have also been used to predict treatment outcome in head and neck cancer [26]. The objective of the present study was to determine if DCE-MRI using clinically approved gadolinium-based contrast agents could be used to detect the microvascular response of SCCHN xenografts to VDA therapy. Enhancement patterns of untreated FaDu xenografts were visualized and quantified after injection of gadofosveset. In untreated control FaDu xenografts, gadofosveset administration resulted in a higher and prolonged tumor enhancement compared to gadopentetate (supplementary figure S2). This is consistent with a previous observation by Farace *et al.*, in which higher enhancement was observed in prostate tumors with gadofosveset compared to gadopentetate [27].

Malignancies of the upper aerodigestive tract often result in significant functional morbidities in patients. These co-morbidities associated with head and neck cancers highlight the need for developing targeted therapies that could potentially increase the therapeutic response without increasing toxicity [28]. In humans, SCCHN are often well vascularized tumors and as a result, there has been active investigation into the therapeutic potential of targeting the angiogenic process in SCCHN [2-4, 6-9]. However, a majority of these studies have utilized monoclonal antibodies or receptor tyrosine kinase inhibitors for inhibiting angiogenesis. Only a few studies have examined the potential of vascular disrupting agents against head and neck cancers [29-31). Although both AIs and VDAs target the tumor vasculature, fundamental differences exist between the two approaches [10, 32, 33]. While AIs typically target mediators of angiogenesis (vascular endothelial growth factor, platelet derived growth factor etc), VDAs target the endothelium either directly or through induction of vasoactive mediators [32, 33]. VDAs induce structural damage to the endothelial cytoskeleton which in turn leads to catastrophic vascular disruption. In contrast to antiangiogenic agents which often require chronic administration for sustained inhibition of angiogenesis, VDAs result in acute changes in permeability leading to thrombosis and cessation of blood flow [30, 34, 35].

In the present study, we examined the ability of DCE-MRI using gadofosveset to detect changes in tumor vascular function of SCCHN xenografts following VDA therapy. Tumor-bearing animals were imaged before and 24h after treatment with a tumor vascular disrupting agent, DMXAA [36]. Gadofosveset-enhanced MRI was sensitive in detecting treatment-induced changes in vascular function. A significant reduction in contrast enhancement was seen following VDA treatment compared to baseline measures indicative of treatment-induced reduction in blood flow. We also observed a good correlation between the early vascular response to therapy (at 24h) with subsequent treatment outcome (d10 tumor response).

Gadopentetate is widely used as a contrast agent for DCE-MRI studies in patients. However, it is limited in its performance due to rapid clearance from the blood. While measurement of enhancement parameters (AUC, amplitude etc) is simple, interpretation of changes in these parameters in the context of underlying physiological changes is complex since they do not distinguish between changes in permeability and perfusion [11, 12, 23]. Clinical trials of antivascular agents using DCE-MRI studies carried out using Gd-DTPA have revealed encouraging results [37, 38]. However, interpretation of DCE-MRI data is complicated by the fact that VDAs exhibit significant effects on perfusion and permeability of tumors [37-39]. Since microvascular permeability is influenced by the physical characteristics of the solute, preclinical studies have suggested that the use of intermediate or large molecular weight (blood pool) contrast agents are likely to provide accurate estimates of changes in blood volume and permeability [40, 41].

The gadolinium-based contrast agent, gadofosveset (Ablavar), is FDA-approved for clinical use for MR angiography (MRA) applications and has been shown to have a higher relaxivity than Gd-DTPA [27, 42]. While the agent is comparable in molecular weight to Gd-DTPA, the agent reversibly binds to serum albumin acting as a blood pool agent. The kinetics of the unbound form is similar to Gd-DTPA. In the present study, differentiation of pharmacokinetics of the unbound and bound forms of Ablavar was not performed. Instead, the change in longitudinal relaxation rate of tumors was used as a quantitative measure of contrast agent concentration. Turetschek et al., have previously reported poor correlation between enhancement parameters and histological tumor grade and microvessel counts in breast tumors [43]. However, in our study, a significant reduction in enhancement parameters, AUC and amplitude, was seen following VDA therapy in SCCHN xenografts.

Finally, CE-US was used to monitor and quantify tumor response to VDA therapy. US imaging offers a relatively inexpensive alternative to advanced imaging techniques such as MRI and CT for non-invasive imaging of tumor growth and vascular function [16, 17]. The use of microbubbles which typically range in the order of a few microns considerably enhances the image contrast and diagnostic utility of US [17]. These microbubbles enhance the acoustic signal of blood thereby enabling non-invasive assessment of tissue perfusion in tissues of interest including tumors. Studies have previously shown the utility of CE-US in determining tumor response to antiangiogenic and antivascular therapy [44, 45]. The results of our study demonstrate that contrast-enhanced microultrasound using non-targeted microbubbles can successfully detect early vascular changes in the tumor following VDA therapy in SCCHN xenografts.

In conclusion, the results of our study provide *in vivo* evidence of the vascular disruptive effects of DMXAA against human SCCHN xenografts. The findings of our study demonstrate the both CE-MRI and CE-US parameters are sensitive in detecting early functional alterations in tumors following VDA therapy *in vivo*. While the activity of the VDA DMXAA has been demonstrated in a number of experimental solid tumor models, to the best of our knowledge, this is the first report demonstrating potent vascular disruption with VDA in SCCHN xenografts derived from surgical human tumor tissue.

In today's era of molecular medicine, imaging techniques play a significant role as investigative tools, particularly in early phase clinical trials for the assessment of targeted anticancer therapeutics. Imaging-based assessment of changes in CE-MRI and CE-US parameters could therefore potentially guide the scheduling and interval of administration of VDA and cytotoxic chemotherapy [46]. The true clinical application of vascular-targeted therapies lies in combination with traditional therapies such as chemotherapy and radiation. So, a study investigating the activity of VDA in combination with chemotherapy would provide useful insight into the optimal timing of vascular function assessment in patients.

Supplementary Material

Refer to Web version on PubMed Central for supplementary material.

Acknowledgments

The authors would like to thank Mr. Steve Turowski and Ms. Jaimee Lockwood for their assistance in performing the imaging studies. This work was supported by grants from the National Cancer Institute R21CA133688 (M.S.) and utilized core resources supported by RPCI's Cancer Center Support Grant from the NCI P30CA16056 (Trump, DL).

Abbreviations

CE-MRI	Contrast-enhanced Magnetic resonance imaging
CE-US	contrast-enhanced ultrasound
SCCHN	squamous cell carcinoma xenografts
VDA	vascular disrupting agent
DMXAA	5,6-dimethylxanthenone-4-acetic acid

REFERENCES

1. Davies L, Welch HG. Epidemiology of head and neck cancer in the United States. Otolaryngol Head Neck Surg. 2006; 135:451–7. [PubMed: 16949981]

2. Gleich LL, Biddinger PW, Pavelic ZP, Gluckman JL. Tumor angiogenesis in T1 oral cavity squamous cell carcinoma: role in predicting tumor aggressiveness. Head Neck. 1996; 18:343–346. [PubMed: 8780945]

3. Hasina R, Whipple ME, Martin LE, Kuo WP, Ohno-Machado L, Lingen MW. Angiogenic heterogeneity in head and neck squamous cell carcinoma: biological and therapeutic implications. Lab Invest. 2008; 88:342–353. [PubMed: 18283272]

4. Galmarini FC, Galmarini CM, Sarchi MI, Abulafia J, Galmirini D. Heterogeneous distribution of tumor blood supply affects the response to chemotherapy in patients with head and neck cancer. Microcirculation. 2000; 7:405–410. [PubMed: 11142337]

5. Kaanders JH, Wijffels KI, Marres HA, Ljungkvist AS, Pop LA, van den Hoogen FJ, de Wilde PC, Bussink J, Raleigh JA, van der Kogel AJ. Pimonidazole binding and tumor vascularity predict for treatment outcome in head and neck cancer. Cancer Res. 2002; 62:7066–7074. [PubMed: 12460928]

6. Bozec A, Sudaka A, Fischel JL, Brunstein MC, Etienne-Grimaldi MC, Milano G. Combined effects of bevacizumab with erlotinib and irradiation: a preclinical study on a head and neck cancer orthotopic model. Br J Cancer. 2008; 99:93–99. [PubMed: 18577994]

7. Fujita K, Sano D, Kimura M, Yamashita Y, Kawakami M, Ishiguro Y, Nishimura G, Matsuda H, Tsukuda M. Anti-tumor effects of bevacizumab in combination with paclitaxel on head and neck squamous cell carcinoma. Oncol Rep. 2007; 18:47–51. [PubMed: 17549344]

8. Bernier J. A multidisciplinary approach to squamous cell carcinomas of the head and neck: an update. Curr Opin Oncol. 2008; 20:249–255. [PubMed: 18391622]

9. Machiels JP, Henry S, Zanetta S, Kaminsky MC, Michoux N, Rommel D, Schmitz S, Bompas E, Dillies AF, Faivre S, Moxhon A, Duprez T, Guigay J. Phase II study of sunitinib in recurrent or metastatic squamous cell carcinoma of the head and neck: GORTEC 2006-01. J Clin Oncol. 2010; 28:21–28. [PubMed: 19917865]

10. Tozer GM, Kanthou C, Baguley BC. Disrupting tumour blood vessels. Nat Rev Cancer. 2005; 5:423–435. [PubMed: 15928673]

11. O'Connor JP, Jackson A, Parker GJ, Jayson GC. DCE-MRI biomarkers in the clinical evaluation of antiangiogenic and vascular disrupting agents. Br J Cancer. 2007; 96:189–195. [PubMed: 17211479]

12. Hylton N. Dynamic contrast-enhanced magnetic resonance imaging as an imaging biomarker. J Clin Oncol. 2006; 24:3293–3298. [PubMed: 16829653]

13. Padhani, AR.; Choyke, PL. New techniques in oncologic imaging. Taylor and Francis; New York: 2006. p. 257-269.

14. Koh DM, Collins DJ. Diffusion-weighted MRI in the body: applications and challenges in oncology. AJR Am J Roentgenol. 2007; 188:1622–1635. [PubMed: 17515386]

15. Seshadri M, Merzianu M, Tang H, Rigual NR, Sullivan M, Loree TR, Popat SR, Repasky EA, Hylander BL. Establishment and characterization of patient tumor-derived head and neck squamous cell carcinoma xenografts. Cancer Biol Ther. 2009; 8:2275–2283. [PubMed: 19829072]

16. Korpanty G, Carbon JG, Grayburn PA, Fleming JB, Brekken RA. Monitoring response to anticancer therapy by targeting microbubbles to tumor vasculature. Clin Cancer Res. 2007; 13:323–330. [PubMed: 17200371]

17. Sullivan JC, Wang B, Boesen EI, D'Angelo G, Pollock JS, Pollock DM. Novel use of ultrasound to examine regional blood flow in the mouse kidney. Am J Physiol Renal Physiol. 2009; 297:F228–F235. [PubMed: 19420115]

18. Hanahan D, Weinberg RA. The hallmarks of cancer. Cell. 2000; 100:57–70. [PubMed: 10647931]

19. Folkman J. Angiogenesis: an organizing principle for drug discovery? Nat Rev Drug Discov. 2007; 6:273–286. Review. [PubMed: 17396134]

20. Yanagi Y, Asaumi J, Unetsubo T, Ashida M, Takenobu T, Hisatomi M, Matsuzaki H, Konouchi H, Katase N, Nagatsuka H. Usefulness of MRI and dynamic contrast-enhanced MRI for differential diagnosis of simple bone cysts from true cysts in the jaw. Oral Surg Oral Med Oral Pathol Oral Radiol Endod. 2010; 110:364–369. [PubMed: 20727497]

21. Unetsubo T, Konouchi H, Yanagi Y, Murakami J, Fujii M, Matsuzaki H, Hisatomi M, Nagatsuka H, Asaumi J. Dynamic contrast-enhanced magnetic resonance imaging for estimating tumor

proliferation and microvessel density of oral squamous cell carcinomas. Oral Oncol. 2009; 45:621–626. [PubMed: 19027349]

22. Newbold K, Castellano I, Charles-Edwards E, Mears D, Sohaib A, Leach M, Rhys-Evans P, Clarke P, Fisher C, Harrington K, Nutting C. An exploratory study into the role of dynamic contrast-enhanced magnetic resonance imaging or perfusion computed tomography for detection of intratumoral hypoxia in head-and-neck cancer. Int J Radiat Oncol Biol Phys. 2009; 74:29–37. [PubMed: 19036529]
23. Hayes C, Padhani AR, Leach MO. Assessing changes in tumour vascular function using dynamic contrast-enhanced magnetic resonance imaging. NMR Biomed. 2002; 15:154–163. [PubMed: 11870911]
24. Kim S, Quon H, Loevner LA, Rosen MA, Dougherty L, Kilger AM, Glickson JD, Poptani H. Transcytolemmal water exchange in pharmacokinetic analysis of dynamic contrast-enhanced MRI data in squamous cell carcinoma of the head and neck. J Magn Reson Imaging. 2007; 26:1607–1617. [PubMed: 17968962]
25. Van Cann EM, Rijpkema M, Heerschap A, van der Bilt A, Koole R, Stoelinga PJ. Quantitative dynamic contrast-enhanced MRI for the assessment of mandibular invasion by squamous cell carcinoma. Oral Oncol. 2008; 44:1147–1154. [PubMed: 18485797]
26. Cao Y, Popovtzer A, Li D, Chepeha DB, Moyer JS, Prince ME, Worden F, Teknos T, Bradford C, Mukherji SK, Eisbruch A. Early prediction of outcome in advanced head-and-neck cancer based on tumor blood volume alterations during therapy: a prospective study. Int J Radiat Oncol Biol Phys. 2008; 72:1287–1290. [PubMed: 19028268]
27. Farace P, Merigo F, Fiorini S, Nicolato E, Tambalo S, Daducci A, Degrassi A, Sbarbati A, Rubello D, Marzola P. DCE-MRI using small-molecular and albumin-binding contrast agents in experimental carcinomas with different stromal content. Eur J Radiol. May 12.2009 2009 [Epub ahead of print].
28. Forastiere AA, Goepfert H, Maor M, Pajak TF, Weber R, Morrison W, Glisson B, Trotti A, Ridge JA, Chao C, Peters G, Lee DJ, Leaf A, Ensley J, Cooper J. Concurrent chemotherapy and radiotherapy for organ preservation in advanced laryngeal cancer. N Engl J Med. 2003; 349:2091–2098. [PubMed: 14645636]
29. Siemann DW, Rojiani AM. The vascular disrupting agent ZD6126 shows increased antitumor efficacy and enhanced radiation response in large, advanced tumors. Int J Radiat Oncol Biol Phys. 2005; 62:846–853. [PubMed: 15936569]
30. Seshadri M, Toth K. Acute vascular disruption by 5,6-dimethylxanthenone-4-acetic acid in an orthotopic model of human head and neck cancer. Transl Oncol. 2009; 2:121–127. 2009. [PubMed: 19701496]
31. Yeung SC, She M, Yang H, Pan J, Sun L, Chaplin D. Combination chemotherapy including combretastatin A4 phosphate and paclitaxel is effective against anaplastic thyroid cancer in a nude mouse xenograft model. J Clin Endocrinol Metab. 2007; 92:2902–2909. [PubMed: 17550961]
32. McKeage MJ, Baguley BC. Disrupting established tumor blood vessels: an emerging therapeutic strategy for cancer. Cancer. 2010; 116:1859–1871. Review. [PubMed: 20166210]
33. Kelland LR. Targeting established tumor vasculature: A novel approach to cancer treatment. Curr Cancer Ther Rev. 2005; 1:1–9.
34. McPhail LD, Griffiths JR, Robinson SP. Assessment of tumor response to the vascular disrupting agents 5,6-dimethylxanthenone-4-acetic acid or combretastatin-A4-phosphate by intrinsic susceptibility magnetic resonance imaging. Int J Radiat Oncol Biol Phys. 2007; 69:1238–1245. [PubMed: 17967313]
35. Ching L-M, Zwain S, Baguley BC. Relationship between tumour endothelial cell apoptosis and tumour blood flow shutdown following treatment with the antivascular agent DMXAA in mice. Br J Cancer. 2004; 90:906–910. [PubMed: 14970872]
36. McKeage MJ, Fong P, Jeffery M, Baguley BC, Kestell P, Ravic M, Jameson MB. 5,6-Dimethylxanthenone-4-acetic acid in the treatment of refractory tumors: a phase I safety study of a vascular disrupting agent. Clin Cancer Res. 2006; 12:1776–1784. [PubMed: 16551862]
37. Galbraith SM, Rustin GJ, Lodge MA, Taylor NJ, Stirling JJ, Jameson M, Thompson P, Hough D, Gumbrell L, Padhani AR. Effects of 5,6-dimethylxanthenone-4-acetic acid on human tumor

microcirculation assessed by dynamic contrast-enhanced magnetic resonance imaging. J Clin Oncol. 2002; 20:3826–3840. [PubMed: 12228202]

38. Galbraith SM, Maxwell RJ, Lodge MA, Tozer GM, Wilson J, Taylor NJ, Stirling JJ, Sena L, Padhani AR, Rustin GJ. Combretastatin A4 phosphate has tumor antivascular activity in rat and man as demonstrated by dynamic magnetic resonance imaging. J Clin Oncol. 2003; 21:2831–2842. [PubMed: 12807936]
39. Zweifel M, Padhani AR. Perfusion MRI in the early clinical development of antivascular drugs: decorations or decision making tools? Eur J Nucl Med Mol Imaging. 2010; 37:S164–S182. [PubMed: 20461374]
40. Bentzen L, Vestergaard-Poulsen P, Nielsen T, Overgaard J, Bjørnerud A, Briley-Saebø K, Horsman MR, Ostergaard L. Intravascular contrast agent-enhanced MRI measuring contrast clearance and tumor blood volume and the effects of vascular modifiers in an experimental tumor. Int J Radiat Oncol Biol Phys. 2005; 61:1208–1215. [PubMed: 15752903]
41. Seshadri M, Bellnier DA, Cheney RT. Assessment of the early effects of 5,6-dimethylxanthenone-4-acetic acid using macromolecular contrast media-enhanced magnetic resonance imaging: ectopic versus orthotopic tumors. Int J Radiat Oncol Biol Phys. 2008; 72:1198–1207. [PubMed: 18954713]
42. Goyen M, Shamsi K, Schoenberg SO. Vasovist-enhanced MR angiography. Eur Radiol. 2006; 16:B9–B14. [PubMed: 16802438]
43. Turetschek K, Floyd E, Helbich T, Roberts TP, Shames DM, Wendland MF, Carter WO, Brasch RC. MRI assessment of microvascular characteristics in experimental breast tumors using a new blood pool contrast agent (MS-325) with 1correlations to histopathology. J Magn Reson Imaging. 2001; 14:237–242. [PubMed: 11536400]
44. O'Connor JP, Carano RA, Clamp AR, Ross J, Ho CC, Jackson A, Parker GJ, Rose CJ, Peale FV, Friesenhahn M, Mitchell CL, Watson Y, Roberts C, Hope L, Cheung S, Reslan HB, Go MA, Pacheco GJ, Wu X, Cao TC, Ross S, Buonaccorsi GA, Davies K, Hasan J, Thornton P, del Puerto O, Ferrara N, van Bruggen N, Jayson GC. Quantifying antivascular effects of monoclonal antibodies to vascular endothelial growth factor: insights from imaging. Clin Cancer Res. 2009; 15:6674–6682. [PubMed: 19861458]
45. Goertz DE, Yu JL, Kerbel RS, Burns PN, Foster FS. High-frequency Doppler ultrasound monitors the effects of antivascular therapy on tumor blood flow. Cancer Res. 2002; 62:6371–6375. [PubMed: 12438217]
46. Masunaga S, Nagasawa H, Nagata K, Suzuki M, Uto Y, Hori H, Kinashi Y, Ono K. Dependency of the effect of a vascular disrupting agent on sensitivity to tirapazamine and gamma-ray irradiation upon the timing of its administration and tumor size, with reference to the effect on intratumor quiescent cells. J Cancer Res Clin Oncol. 2007; 133:47–55. [PubMed: 16924543]

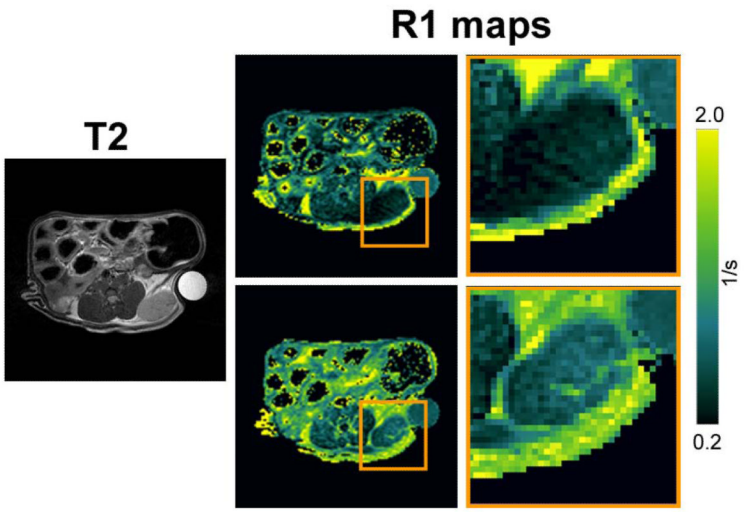

Figure 1. Gadofosveset-enhanced MRI of FaDu SCCHN xenografts

Axial T2W image and corresponding pseudo-colorized R1-maps (R1=1/T1) a mouse bearing FaDu SCCHN xenograft (box) before (*top panel*) and after (*bottom panel*) gadofosveset administration. Enlarged ROI of the tumor is also shown.

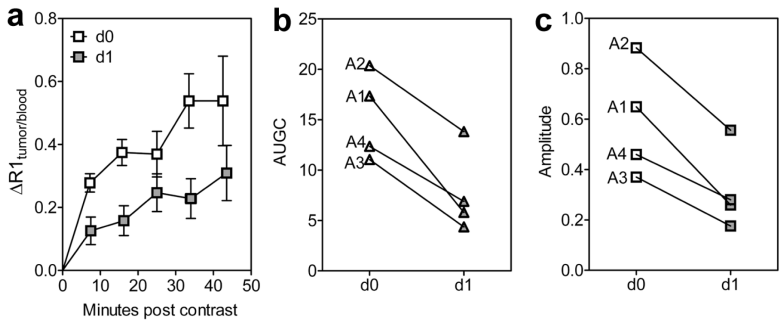

Figure 2. Gadofosveset-enhanced MRI of FaDu SCCHN response to VDA therapy

Change in normalized R1 (ΔR1tumor/blood; (a), area under the gadolinium concentration curve (AUGC; b) and amplitude (max. ΔR1; c) of FaDu tumors before (day 0) and after VDA treatment (day 1). A consistent and significant ($p<0.05$) reduction in AUGC and amplitude was observed following VDA treatment compared to pretreatment estimates in all four tumors.

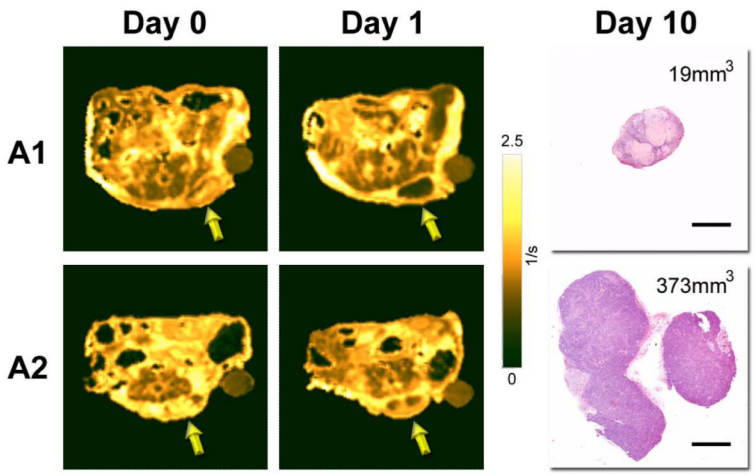

Figure 3. Early vascular response to VDA therapy correlates with treatment outcome

The panel of images shown in the figure represent post contrast R1 maps of two tumors (A1 and A2) on day 0 and day 1 along with corresponding H&E sections (bar = 2mm). Tumor A1 showed ~68% reduction in AUGC at 24 hours post VDA therapy and was associated with marked tumor growth inhibition (19 mm^3 on day 10). Histologic examination of the tumor also showed extensive areas of necrosis. In contrast, tumor A2 showed only ~35% reduction in AUGC at 24 hours compared to baseline values and was associated with tumor growth (373.7 mm^3 on day 10). Histologic sections of the tumor showed the presence of a viable proliferating tumor mass with minimal areas of necrosis. Histologic sections of all 4 treated tumors are shown in supplementary material (S1).

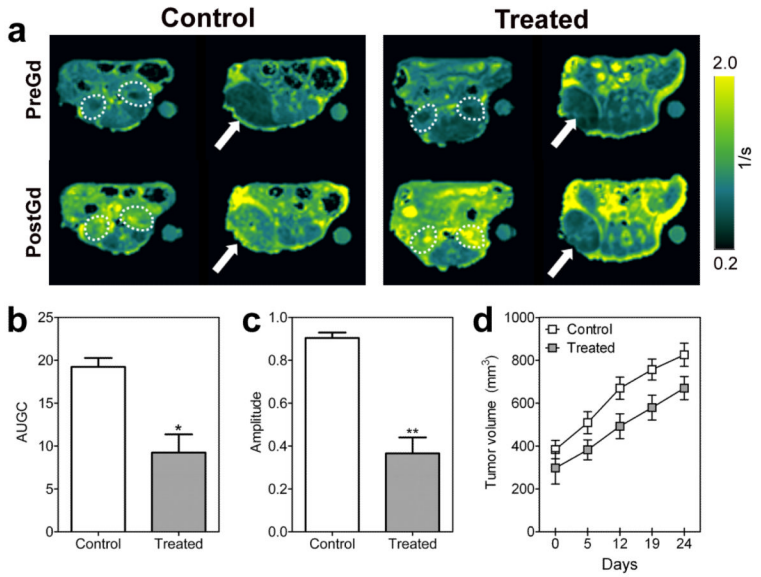

Figure 4. DCE-MRI of vascular disruption in patient tumor-derived SCCHN xenografts

(A) Panel of images represent R1 maps of control and VDA-treated SCID mice bearing patient tumor-derived SCCHN xenografts before (PreGd) and after gadofosveset injection (PostGd). Two contiguous slices showing kidneys (slice 1, *dotted outline*) and tumors (*arrow*) are shown. In contrast to control tumors, VDA-treated tumors showed a reduction in enhancement following contrast agent injection.

Bar graphs showing the area under the curve (AUC; b), amplitude ($\Delta R1_{max}$; c) and tumor growth curves (d) of control and VDA-treated SCCHN xenografts. A significant reduction in AUC ($p<0.05$) and amplitude ($p<0.01$) was observed 24 hours after VDA therapy (n=4) compared to untreated controls (n=3).

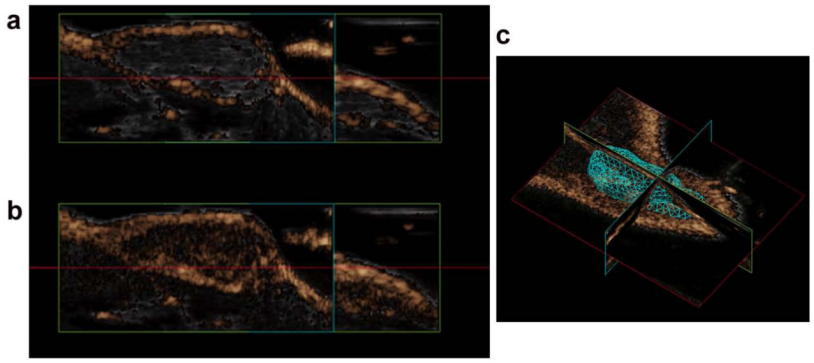

Figure 5. Contrast-enhanced US of patient tumor-derived SCCHN xenografts

Non linear contrast mode images (copper overlay) of a control SCCHN xenograft before and after administration of microbubbles. Administration of the microbubbles resulted in ~50% increase in non linear contrast model signal (Fig 5b; PA = 76.63%) compared to precontrast estimates (Fig 5a; PA = 26.62%). Corresponding 3D volume generated for the tumor is shown in Figure 5c (119 mm^3).

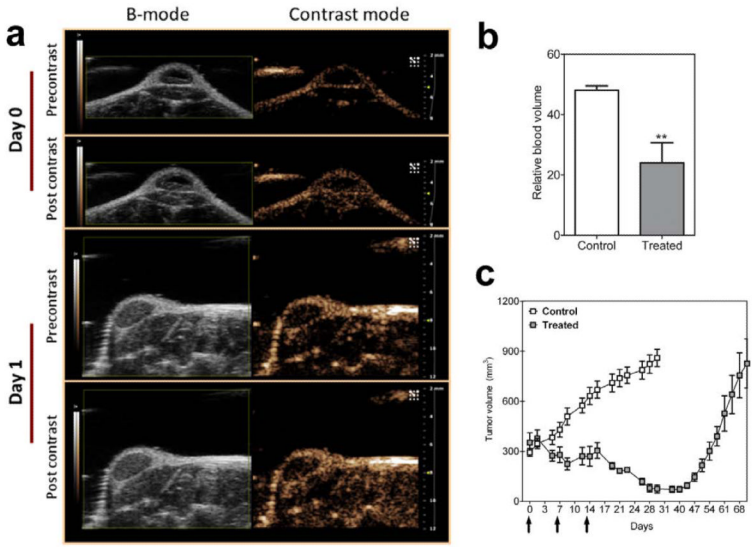

Figure 6. CE-US of patient tumor-derived SCCHN response to VDA therapy

(a) B-mode images and contrast mode images of an SCCHN xenograft derived from human surgical tissue before (day 0) and after VDA treatment (day 1). Images were obtained prior to and following administration of non-targeted microbubbles to estimate tumor enhancement. (b) Relative blood volume (rBV) measurements obtained from CE-US in control (n=7) and VDA-treated (n=4) SCCHN xenografts. A significant reduction in blood volume ($p<0.01$) indicative of tumor vascular disruption was observed. (c) VDA treatment at this dose (once a week x 3) resulted in a significant delay in tumor regrowth *in vivo* (arrows indicate days of VDA treatment).